Elucidating the acid-base mechanisms underlying otolith overgrowth in fish exposed to ocean acidification

Garfield T. Kwan[1,2]*, Martin Tresguerres[1]*

[1]Marine Biology Research Division, Scripps Institution of Oceanography, University of California San Diego, USA

[2]NOAA Fisheries Service, Southwest Fisheries Science Center, USA

*Corresponding authors: gkwan@ucsd.edu; mtresguerres@ucsd.edu

Abstract

Over a decade ago, ocean acidification (OA) exposure was reported to induce otolith overgrowth in teleost fish. This phenomenon was subsequently confirmed in multiple species; however, the underlying physiological causes remain unknown. Here, we report that splitnose rockfish (*Sebastes diploproa)* exposed to ~1,600 µatm pCO_2 (pH ~7.5) were able to fully regulated the pH of both blood and endolymph (the fluid that surrounds the otolith within the inner ear). However, while blood was regulated around pH 7.80, the endolymph was regulated around pH ~8.30. These different pH setpoints result in increased pCO_2 diffusion into the endolymph, which in turn leads to proportional increases in endolymph [HCO_3^-] and [CO_3^{2-}]. Endolymph pH regulation despite the increased pCO_2 suggests enhanced H^+ removal. However, a lack of differences in inner ear bulk and cell-specific Na^+/K^+-ATPase and vacuolar type H^+-ATPase protein abundance localization pointed out to activation of preexisting ATPases, non-bicarbonate pH buffering, or both, as the mechanism for endolymph pH-

regulation. These results provide the first direct evidence showcasing the acid-base chemistry of the endolymph of OA-exposed fish favors otolith overgrowth, and suggests that this phenomenon will be more pronounced in species that count with more robust blood and endolymph pH regulatory mechanisms.

Keywords

Endolymph, climate change, calcification, biomineralization, rockfish, carbon dioxide

Introduction

The inner ear of teleost fishes contains three pairs of otoliths that contribute to hearing and maintaining balance. Otoliths are comprised of calcium carbonate ($CaCO_3$) embedded within a protein matrix, and are biomineralized within an acellular fluid called the endolymph (Payan et al., 2004a). Otoliths are biomineralized in a successive ring pattern correlated with the fish growth rate (Campana and Neilson, 1985; Kalish, 1989; Pannella, 1971), which are used by scientists and fishery managers to estimate fish age and length (Campana, 2001; Campana and Thorrold, 2001), estimate recruitment, and set fishery-specific catch limits (Methot, 2015; Vitale et al., 2019).

Originally, it was predicted that CO_2-induced ocean acidification (OA) would impair otolith biomineralization because the associated decreases in seawater pH and $[CO_3^{2-}]$ hamper $CaCO_3$ precipitation (Ishimatsu et al., 2008). However, subsequent studies reported that fish exposed to OA developed enlarged otoliths (S. Bignami et al., 2013; Sean Bignami et al., 2013; Checkley et al., 2009; Faria et al., 2017; Hurst et al., 2012; Réveillac et al., 2015; Shen et al., 2016). These findings led to a broader

awareness that otolith biomineralization is strongly linked to endolymph and blood chemistries, and to the hypothesis that biological regulation of endolymph pH could lead to increased [CO_3^{2-}] resulting in otolith overgrowth (Checkley et al., 2009). In addition, fish exposed to hypercapnia typically accumulate [HCO_3^-] in their plasma to compensate the respiratory acidosis; this could result in enhanced HCO_3^- flux into the endolymph and further contribute to otolith overgrowth (Heuer and Grosell, 2014). However, experimental support for these hypotheses is lacking, as there are no reports of endolymph acid-base parameters under OA-relevant conditions, and only a few studies have measured blood acid-base parameters in fish exposed to OA-relevant CO_2 levels (Esbaugh et al., 2016, 2012; Montgomery et al., 2019). This knowledge gap is in large part due to the disrupting effects of blood sampling by caudal puncture on the acid-base status of fish internal fluids and the challenge of blood vessel cannulation in small fish and species with convoluted dorsal aorta anatomy, coupled with the difficulty of collecting sufficient endolymph for analyses. Moreover, the cellular heterogeneity of the inner ear complicates the quantification of ionocyte-specific responses using standard molecular and biochemical assays on bulk tissue. As a result, the underlying acid-base and physiological causes of OA-induced otolith overgrowth remain unknown.

The chemistry of the endolymph is actively controlled by the inner ear epithelium to maintain acid-base conditions that promote biomineralization, namely, higher pH, [HCO_3^-], [CO_3^{2-}], and total CO_2 than the blood (Payan et al., 1999, 1997; Takagi, 2002; Takagi et al., 2005). This gradient is actively maintained by two types of ion-transporting cells ("ionocytes"): the Type-I ionocyte, which transports K^+ and Cl^- into the endolymph and removes H^+ powered by Na^+/K^+-ATPase (NKA) (Kwan et al., 2020; Mayer-Gostan

et al., 1997; Payan et al., 1997; Takagi, 1997) and the Type-II ionocyte, which secretes HCO_3^- into the endolymph driven by V-type H^+-ATPase (VHA) (Kwan et al., 2020; Mayer-Gostan et al., 1997; Payan et al., 1997; Takagi, 1997; Tohse et al., 2006, 2004). However numerous other cells within the inner ear organ also express NKA and VHA, including the sensory hair cells and the endothelial cells that make up the blood vessels (Kwan et al., 2020; Mayer-Gostan et al., 1997; Shiao et al., 2005).

In the current study, splitnose rockfish (*Sebastes diploproa)* were exposed to ~1,600 µatm CO_2 (pH ~7.5), a condition readily experienced in their natural habitat (Culberson and Pytkowicz, 1970; Love et al., 2002) and predicted for the surface ocean by the year 2300 (Goodwin et al., 2018). The OA exposure spanned three days, a duration previously documented to result in otolith overgrowth in fish larvae (Faria et al., 2017). Blood acid-base chemistry was measured after taken samples using a benzocaine-based anesthetic protocol that yields measurements comparable to those achieved using cannulation (Montgomery et al., 2019). Additionally, we took advantage of the large rockfish inner ear organ to collect sufficient endolymph for acid-base chemistry analysis, and inner ear tissue for quantification of NKA and VHA protein abundances. Finally, we performed immunohistochemical analyses on six inner ear cell types to explore potential cell-specific changes in protein expression patterns. This multidimensional approach allowed us to explore the mechanistic acid-base causes that underlie otolith overgrowth in fish exposed to OA.

Methods

Specimens

Juvenile splitnose rockfish (*S. diploproa*) were caught from drifting kelp paddies off the shores of La Jolla and raised in the Hubbs Experimental Aquarium (La Jolla, USA) in accordance to the permit (#SCP13227) issued by the California Department of Fish and Wildlife. Rockfish were raised for >2 years in a flow-through system with seawater continuously pumped from the Scripps Coastal Reserve, and were fed frozen market squids and food pellets (EWOS, Cargill Incorporated, Minneapolis, MN, USA). Average rockfish total length (12.33 ± 0.16 cm) and weight (49.11 ± 2.18 g) (N=9) were not significantly different between treatments. All experiments were approved under the Institutional Animal Care and Use Committee protocol (#S10320) by the Scripps Institution of Oceanography, University of California San Diego animal care committee.

Experimental Aquarium Setup

Two header tanks were supplied with ambient seawater from the Scripps Coastal Reserve, one was not manipulated and was considered as the control condition. The other header tank was bubbled with CO_2 using a pH-stat system (IKS Aquastar, Karlsbad, Germany) to maintain a seawater pH ~7.5 and generate the OA condition. Temperature and pH were continuously monitored and recorded every 2 minutes using the IKS Aquastar system (figure S1). Discrete seawater samples were collected from header tanks at the beginning and end of each experiment, and analyzed for alkalinity (via titration with LabView software Version 2.9j; National Instruments, Austin, Texas, United States), pH (using the indicator dye purified m-cresol purple (Liu et al., 2011) in an Agilent 8453 spectrophotometer (Agilent, Santa Clara, CA, USA)), and salinity (by converting density measurements using Mettler Toledo DE-45 (Mettler-Toledo,

Columbus, Ohio, United States)) by the Dickson Lab (Scripps Institution of Oceanography). The pH values from the discrete seawater samples were used to validate and back-correct the IKS pH measurements. Subsequently, the pH, alkalinity, and salinity values were used to calculate pCO_2 using CO2SYS (Lewis and Wallace, 1998). These analyses indicated control pH and pCO_2 levels of 7.89 ± 0.012 and 571.90 ± 4.88 µatm, respectively, which are typical for La Jolla, USA (Frieder et al., 2012; Hofmann et al., 2011; Takeshita et al., 2015). In contrast, pH and pCO_2 in the OA treatment were 7.49 ± 0.01 and 1,591.56 ± 18.58 µatm, respectively (table S1).

Each header tank supplied water to three opaque 3-L experimental tanks at a flow rate of 0.3-L min^{-1}. Individual rockfish were acclimated within an experimental tank for 12 hours, followed by a 72-hour exposure to control or OA conditions. To ensure similar metabolic state among individuals, rockfish were not fed during the 48 hours prior to the acclimations or during the experiment. Three separate experiments were conducted during March 2020, each time with three control and three OA-exposed fish. No mortality was observed.

Blood, endolymph, and inner ear sampling

Sampling and acid-base determinations were performed in a temperature-controlled room at 18°C (i.e. same as that of seawater). Fish were anesthetized by stopping the seawater flow into the individual experimental tank and slowly adding benzocaine through to achieve a final concentration of 0.15 g/L. After fish lost equilibrium (~5 minutes), they were moved to a surgery table where the gills were irrigated with aeriated seawater from their respective treatment (control or OA)

containing benzocaine (0.05 g/L) using a pump (Harter et al., 2021; Montgomery et al., 2019, 2022). Blood was drawn from the caudal vein using a heparinized syringe and pH was immediately measured using a microelectrode (Orion™ PerpHecT™ Ross™, ThermoFisher Scientific, Waltham, MA, USA). Next, blood was centrifuged for 1 minute at 6,000xg using a microcentrifuge (VWR Kinetic Energy 26 Joules, Radnor, PA, USA), and the resulting plasma was measured for total CO_2 (TCO_2) using a carbon dioxide analyzer (Corning 965, Ciba Corning Diagnostic, Halstead, Essex, United Kingdom). After blood sampling (N=8-9), the fish was euthanized by spinal pithing, and the gills were quickly removed. Endolymph (N=7-8) was drawn using a heparinized syringe from the ventral side of the skull, and pH and TCO_2 were measured as described above. CO_2 loss was minimized by measuring endolymph within 3 minutes after spinal pithing. Inner ear tissue was either flash frozen in liquid nitrogen and stored at -80°C, or fixed in 4% paraformaldehyde (8 hours at 4°C), incubated in 50% ethanol (8 hours at 4°C), then stored in 70% ethanol until processing.

HCO_3^-, CO_3^{2-}, and pCO_2 calculation

Blood and endolymph pH and TCO_2 values were used to calculate [HCO_3^-], [CO_3^{2-}], and pCO_2 using the Henderson-Hasselbalch equation. The solubility coefficient of CO_2 (plasma: 0.0578 mmol L^{-1} $Torr^{-1}$; endolymph: 0.0853 mmol L^{-1} $Torr^{-1}$), ionic strength (plasma: 0.15 mol L^{-1}, endolymph: 0.18 mol L^{-1}), pK_1' (plasma: ~6.20, endolymph: ~6.16), and pK_2' (plasma: ~9.76, endolymph: ~9.71) were based upon (Boutilier et al., 1984) and (Takagi, 2002) for blood and endolymph, respectively. The

161 [Na^+] (plasma: 170 mmol L^{-1}, endolymph: 100 mmol L^{-1}) used for calculating pK_1' was
162 based upon (Payan et al., 1997).
163
164 *Antibodies*
165 NKA was immunodetected using a monoclonal α5 mouse antibody raised against
166 the α-subunit of chicken NKA (a5, Developmental Studies Hybridoma Bank, Iowa City,
167 IA, USA; (Lebovitz et al., 1989)), whereas the β-subunit of VHA was immunodetected
168 using a custom-made polyclonal rabbit antibody (epitope: AREEVPGRRGFPGYC;
169 GenScript, Piscataway, USA). These antibodies have been previously used in the inner
170 ear of the Pacific chub mackerel (*Scomber japonicus*; (Kwan et al., 2020)), and were
171 validated here for splitnose rockfish (figure S2). Secondary antibodies goat anti-mouse
172 HRP-linked secondary antibodies (Bio-Rad, Hercules, CA, USA) and goat anti-rabbit
173 HRP-linked secondary antibodies (Bio-Rad) were used for immunoblotting.
174
175 *Western Blotting and Relative Protein Abundance Analysis*
176 Frozen inner ear samples were immersed in liquid nitrogen, pulverized using a
177 handheld motorized homogenizer (Kimble®/Kontes, Dusseldorf, Germany), and
178 suspended in ice-cold homogenization buffer containing protease inhibitors (250 mmol
179 l^{-1} sucrose, 1 mmol l^{-1} EDTA, 30 mmol l^{-1} Tris, 10 mmol l^{-1} benzamidine hydrochloride
180 hydrate, 1 mmol l^{-1} phenylmethanesulfonyl fluoride, 1 mmol l^{-1} dithiothreitol, pH 7.5).
181 Samples were centrifuged at low speed (3,000xg, 10 minutes, 4°C) to remove debris,
182 and the resulting supernatant was considered the crude homogenate. Total protein
183 concentration in all fractions was determined by the Bradford assay (Bradford, 1976).

Prior to SDS-electrophoresis, samples were mixed with an equal volume of 90% 2x Laemmli buffer and 10% β-mercaptoethanol, and heated at 70°C for 5 minutes. Proteins (crude homogenate: 10 µg per lane; membrane-enriched fraction: 5 µg per lane) were loaded onto a 7.5% polyacrylamide mini gel (Bio-Rad, Hercules, CA, USA) – alternating between control and high CO_2 treatments to avoid possible gel lane effects. The gel ran at 200 volts for 40 minutes, and the separated proteins were then transferred to a polyvinylidene difluoride (PVDF) membrane using a wet transfer cell (Bio-Rad) at 100 mAmps at 4°C overnight. PVDF membranes were incubated in tris-buffered saline with 1% tween (TBS-T) with milk powder (0.1 g/mL) at RT for 1 hour, then incubated with primary antibody (NKA: 10.5 ng/ml; VHA: 3 µg/ml) in blocking buffer at 4°C overnight. On the following day, PVDF membranes were washed with TBS-T (three times; 10 minutes each), incubated in blocking buffer with their respective secondary antibodies (1:10,000) at RT for 1 hour, and washed again with TBS-T (three times; 10 minutes each). Bands were made visible through addition of ECL Prime Western Blotting Detection Reagent (GE Healthcare, Waukesha, WI) and imaged and analyzed in a BioRad Universal III Hood using Image Lab software (version 6.0.1; BioRad). Following imaging, the PVDF membrane was incubated in Ponceau stain (10 minutes, room temperature) to estimate protein loading. Relative protein abundance (N=6-8) were quantified using the Image Lab software (version 6.0.1; BioRad) and normalized by the protein content in each lane.

Whole-mount immunohistochemistry and confocal microscopy

Immunolabeling was performed based on the protocol described in Kwan *et al.*, (2020) for tissue sections and optimized for whole tissues as follows. Fixed inner ear tissue was rehydrated in phosphate buffer saline + 0.1% tween (PBS-T) for 10 min. Autofluorescence was quenched by rinsing in ice-cold PBS-T with sodium borohydride (1.5 mg/mL; six times; 10 minutes each), followed by incubation in blocking buffer (PBS-T, 0.02% normal goat serum, 0.0002% keyhole limpet hemocyanin) at room temperature for one hour. Samples were incubated with blocking buffer containing primary antibodies (NKA: 40 ng/mL; VHA: 6 µg/mL) at 4°C overnight. On the following day, samples were washed in PBS-T (three times at room temperature; 10 minutes each), and incubated with the fluorescent secondary antibodies (1:500) counterstained with DAPI (1 µg/mL) at room temperature for 1 hour. Samples were washed again in PBS-T as before and stored at 4°C until imaging.

Immunostained inner ear samples were immersed in PBS-T, mounted onto a depressed glass slide fitted with a glass cover slip (No. 1.5, 0.17 mm) and imaged using a Zeiss LSM800 inverted confocal microscope equipped with a Zeiss LD LCI Plan-Apochromat 40x/1.2 Imm Korr DIC M27 objective and Zeiss ZEN 2.6 blue edition software (Cambridge, United Kingdom). The following channels were used for imaging: VHA (excitation 493 nm with 1% laser power, emission 517 nm, detection 510– 575 nm), NKA (excitation 577 nm at 1% laser power, emission 603 nm, detection 571–617 nm), and DAPI (excitation 353 nm at 0.7% laser power, emission 465 nm, detection 410–470 nm). Z-stacks (range: ~70–400 optical sections; thickness: ~0.27 µm per section) of the various inner ear cell types were visualized as maximum intensity projection, and through orthogonal cuts to capture fluorescent signal across the X-Z and

Y-Z planes. Inner ear organs from four control and four OA-exposed rockfish were imaged.

Statistical Analysis

Normality was tested using the Shapiro-Wilk normality test, and homogeneity was tested using the F-test. Datasets that failed to meet the assumptions of normality were log- (i.e. $[CO_3^{2-}]$, pH) or inverse-transformed (i.e. $[H^+]$). Acid-base parameters were analyzed using two-way analysis of variance (2-way ANOVA), with "CO_2 level" (control or OA) and "internal fluid" (blood or endolymph) as factors. If significant interaction effect was detected, subsequent Tukey honest significant difference (HSD) tests were used. NKA and VHA protein abundances were analyzed using two-tailed Student's t-tests. Values are reported as mean ± s.e.m., and an alpha of 0.05 was employed for all analyses. Statistical tests were performed using Prism (version 7.0a) and R (version 4.0.3; R Development Core Team, 2013).

Results and discussion

The difference in seawater pCO_2 between the control and OA-condition was ~1,000 µatm, which induced an equivalent elevation in blood pCO_2 from 1,603.25 ± 190.69 µatm in control fish to 2,659.20 ± 223.87 µatm in OA-exposed fish (figure 1a). However, blood pH was fully regulated (control: 7.75 ± 0.03; OA: 7.85 ± 0.04) (figure 1b). As is typical for regulation of blood acidosis (Tresguerres and Hamilton, 2017), OA-exposed fish demonstrated a significant accumulation of HCO_3^- in blood plasma, from 2.37 ± 0.20 mM in control fish up to 5.16 ± 0.31 mM in OA-exposed fish (figure 1c). This

response matches the magnitude of the hypercapnic stress according to classic Davenport acid-base physiology, as well as the three previous studies on blood acid-base chemistry in fish exposed to OA-relevant CO_2 levels (Esbaugh et al., 2016, 2012; Montgomery et al., 2019). In addition, the increased plasma TCO_2 at unchanged pH led to the tripling of plasma [CO_3^{2-}] from ~0.02 to ~0.07 mM (figure 1d). These increases in blood [HCO_3^-] and [CO_3^{2-}] may contribute to the skeletal hypercalcification (Di Santo, 2019) and deformities (Pimentel et al., 2014) reported in some OA-exposed fishes.

The endolymph of control rockfish had higher TCO_2 compared to the blood (9.06 ± 0.38 vs 2.46 ± 0.20 mM; figure S3) and also a higher pH (8.32 ± 0.05 vs. 7.75 ± 0.03), resulting in lower pCO_2 (971.38 ± 120.70 vs. 1,603.25 ± 190.69 µatm), higher [HCO_3^-] (8.63 ± 0.35 vs. 2.37 ± 0.20 mM), and much higher [CO_3^{2-}] (0.36 ± 0.04 vs 0.02 ± 0.01 mM) (figure 1a-d). Importantly, these measurements revealed higher pH and lower pCO_2, TCO_2, [HCO_3^-] and [CO_3^{2-}] compared to previous studies that collected endolymph without previously anesthetizing the fish (Payan et al., 1999, 1997), and to others that used 2-phenoxyethanol as anesthetic but did not irrigate the gills during endolymph collection (Takagi, 2002; Takagi et al., 2005) (table S2). This finding highlights the crucial importance of sampling procedures for accurate acid-base measurements in fish physiological fluids. Indeed, fish struggling during handling and hypoxia due to gill collapse during emersion are known to greatly affect blood acid-base measurements, and our results indicate that these disturbances extend to the endolymph.

In rockfish exposed to OA, endolymph pCO_2 increased from 971.38 ± 120.70 to 1503.21 ± 73.72 µatm (figure 1a). Crucially, this ~500 µatm increase was half of that observed in the blood and therefore the pCO_2 difference between blood and endolymph increased from ~600 to ~1,100 µatm, which is predicted to induce a proportional increase in CO_2 flux into the endolymph following Fick's law of diffusion. Endolymph TCO_2 in OA-exposed rockfish also nearly doubled (control: 9.06 ± 0.38 mM; OA= 15.96 ± 1.02 mM; figure S3) and, since pH remained unchanged at ~8.30 pH (figure 1b), it was reflected as increased [HCO_3^-] (control: 8.63 ± 0.35 mM, OA: 15.19 ± 0.95 mM vs) (figure 1c) and [CO_3^{2-}] (control: 0.36 ± 0.04 mM; OA 0.67 ± 0.06 mM) (figure 1d). Since aragonite saturation state ($\Omega_{aragonite}$) is directly proportional to [CO_3^{2-}], it implies that biomineralization in the endolymph of OA-exposed fish is nearly twice more favorable than in that of control fish. To our knowledge, this is the first direct evidence that the acid-base chemistry in the endolymph of OA-exposed fish favors otolith overgrowth.

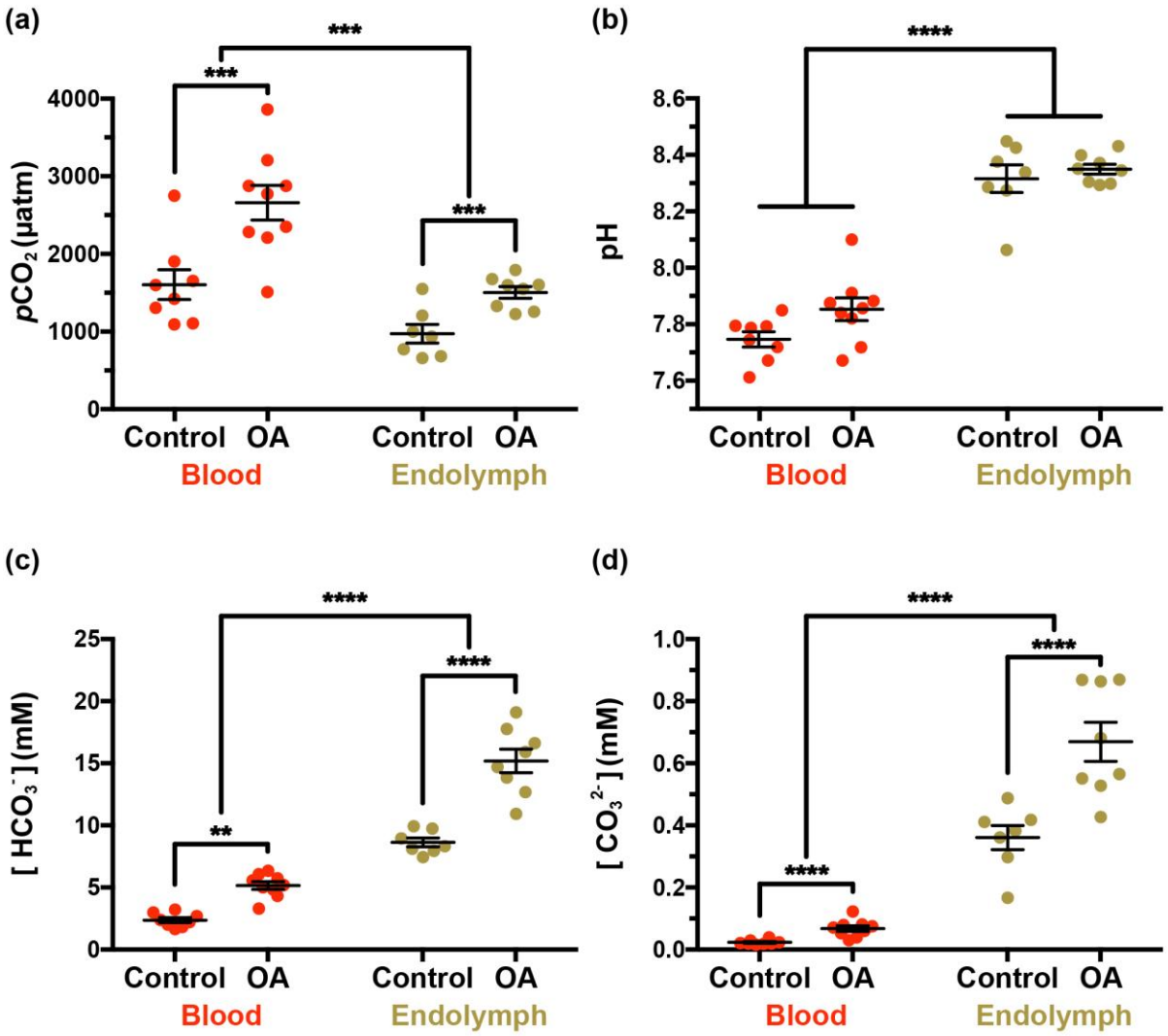

Figure 1: Blood and endolymph acid-base parameters in control and OA-exposed rockfish. **A)** pCO_2, **B)** pH, **C)** $[HCO_3^-]$, and **D)** $[CO_3^{2-}]$. Data is presented as mean and s.e.m. for each group and the individual measurements are shown as red (blood) or beige (endolymph) points (N= 7-9). Statistical significance between fluids, and between treatments for a given fluid are indicated by the connecting lines and asterisks (2-way ANOVA, *p<0.05, **p<0.005, ***p<0.001, ****p<0.0001). Statistical details are reported in tables S3-S5, and TCO_2,$[CO_2]$ and $[H^+]$ are shown in figure S3.

The increased pCO_2 diffusive rate into the endolymph and subsequent generation of H^+ as a result of CO_2 hydration and $CaCO_3$ biomineralization would be expected to induce a decrease in pH. Thus, the lack of change in endolymph pH in OA-exposed rockfish indicates robust pH regulation. Hence, we hypothesized that OA-exposed fish may have increased abundance of NKA and VHA, as these ATPases are proposed to provide the driving force for transepithelial H^+ and HCO_3^- transport across the inner ear epithelium (Kwan et al., 2020; Mayer-Gostan et al., 1997; Payan et al., 1997; Shiao et al., 2005). However, Western blotting on bulk inner ear tissue revealed no significant differences between control and OA-exposed fish (figure 2, table S6).

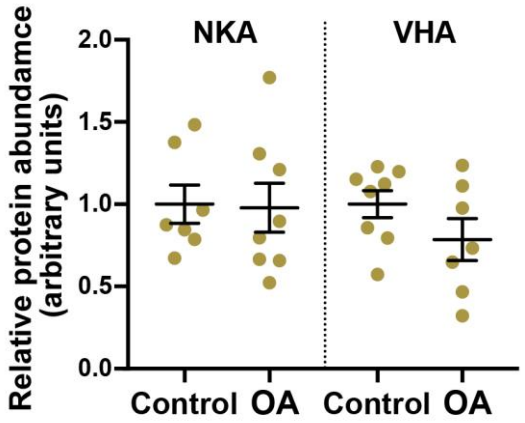

Figure 2: Na^+/K^+-ATPase (NKA) and V-type H^+-ATPase (VHA) protein abundance in the inner ear organ of control and OA-exposed rockfish. Data is presented as mean and s.e.m. and the individual measurements are shown as beige points (N= 7-8). Relative protein abundance was calculated for each ATPase; NKA and VHA abundances are not comparable to each other. There were no significant differences for NKA (p=0.9104) or VHA (p=0.1695). Statistical details are reported in tables S6.

315 Next, we used immunocytochemistry and confocal microscopy to examine
316 potential changes in NKA and VHA abundance or sub-cellular localization in specific
317 inner ear epithelial cell types. The NKA and VHA immunostaining in rockfish inner ear
318 epithelial cells generally matched reports from other fish species (Kwan et al., 2020;
319 Pisam et al., 1998; Shiao et al., 2005; Takagi, 1997) (figure 3; figure S4), and there
320 were no apparent differences between control and OA-exposed fish in any cell type in
321 terms of signal intensity of subcellular localization. The Type-I ionocytes are
322 characterized by intense NKA signal in their highly infolded basolateral membrane and
323 by a much fainter cytoplasmic VHA signal (figure 3a). These ionocytes are most
324 abundant in the meshwork area, where they contact each other by their pseudopods
325 giving the appearance of an interconnected matrix. The Type-II ionocytes are
326 interspersed between the Type-I ionocytes in the meshwork area and have cytoplasmic
327 VHA signal of comparable intensity to that in the Type-I ionocytes; however, they lack
328 NKA signal (figure 3a). The sensory hair cells are in the macula; they express intense
329 NKA signal in their basolateral membrane and very intense cytoplasmic VHA signal,
330 which was especially concentrated towards their basal area consistent with synaptic
331 vesicles (figure 3b). The supporting cells surround each sensory hair cell; they display
332 faint cytoplasmic VHA signal and no detectable NKA signal (figure 3b). The granular
333 cells flank the macula and have a characteristic columnar shape. These cells have faint
334 NKA signal along their lateral plasma membrane and faint cytoplasmic VHA signal
335 (figure 3c). Finally, the squamous cells are found in the patches area in the distal side of
336 the epithelium; these cells are very thin and have NKA signal on their ribbon-like lateral

membrane as well as faint cytoplasmic VHA signal (figure 3d). A summary of the NKA and VHA relative signal intensities in each cell type is reported in table S7.

The lack of apparent differences in NKA and VHA abundance and localization cellular patterns between control and OA-exposed fish indicates that preexisting levels of NKA and VHA were sufficient to mediate the endolymph pH regulation observed in our study. Overall, these findings are consistent with models suggesting that H^+ extrusion from the endolymph into the blood passively follows the transepithelial potential that is established by active K^+ excretion into the endolymph (Payan et al., 2004). And since the function of the sensory hair cells requires a high [K^+] in the endolymph, modulation of inner ear transepithelial potential for the sole purpose of decreasing H^+ extrusion seems unlikely.

In our recent paper (Kwan et al., 2020), we proposed that HCO_3^- transport into the endolymph and H^+ removal could be upregulated by insertion of VHA into the basolateral membrane of Type-II ionocytes; however, we found no evidence for such mechanism in OA-exposed rockfish (figure 3a, *right panels*). Instead, upregulation of ATPase activity could have occurred *via* other post-translational modifications or by increased substrate availability (c.f. Kwan et al., 2021). The expression of carbonic anhydrases, ion exchangers, and other acid-base relevant proteins must be examined in future studies, ideally through an approach that includes cell-specific analyses. Lastly, a contribution of non-bicarbonate buffering to endolymph pH regulation cannot be ruled out; unfortunately, performing the required titrations are not trivial due to the small volume of this fluid.

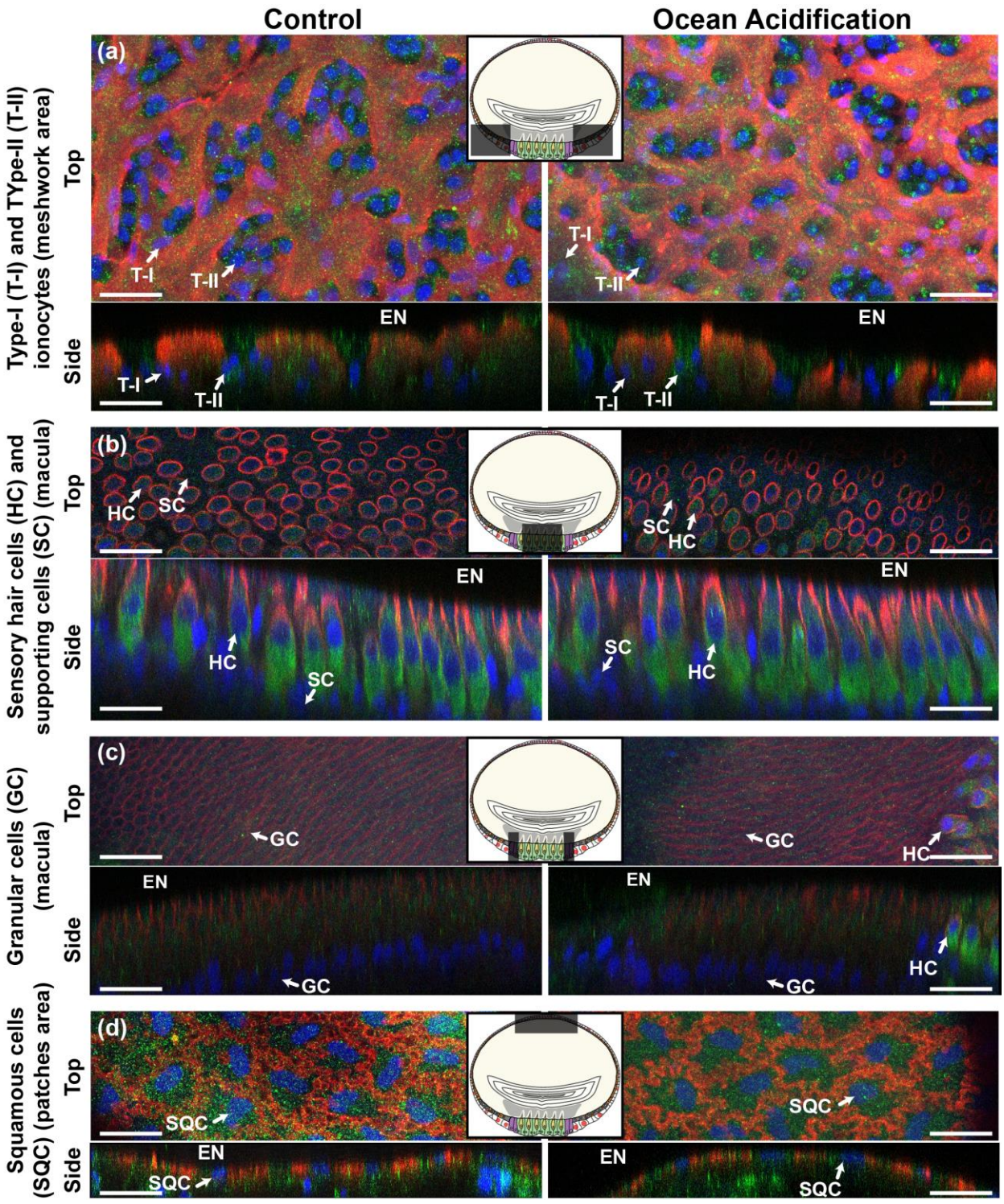

Figure 3: Immunocytochemistry of the inner ear epithelium of control and OA-exposed rockfish. Na^+/K^+-ATPase is in red, V-type H^+-ATPase is in green, and nuclei are in blue. There were no apparent differences in NKA or VHA signal intensities or localization

patterns between control and OA-exposed fish. **(a)** Type-I (T-I) and Type-II ionocytes (T-II), **(b)** sensory hair cells (HC) and supporting cells (SC), **(c)** granular cells (GC), and **(d)** squamous cells (SQC). The top view shows the X-Y plane in maximum projection, whereas the side view shows the X-Z or Y-Z plane using orthogonal cuts. EN = endolymph. Scale bar = 20 μm. Images are representative of inner ear from four control and four OA-exposed rockfish. The shaded boxes in the diagrams indicate the location of each cell type within the otolith sac. A larger diagram showcasing the heterogeneous cellular anatomy of the inner ear epithelium is provided in figure S4.

Conclusions

Increased endolymph [HCO_3^-] and [CO_3^{2-}] provides a mechanistic explanation for otolith overgrowth in OA-exposed fish, a phenomenon that was first described over a decade ago (Checkley et al., 2009). The ultimate cause is an interplay between blood and endolymph acid-base regulation, which results in increased CO_2 flux into the endolymph coupled with endolymph pH regulation. As a result, the carbonate equilibria reactions shift to the right, promoting [HCO_3^-] and [CO_3^{2-}] accumulation bound to increase $\Omega_{aragonite}$, and thus promote biomineralization (figure 4). This implies that otolith overgrowth in response to OA will be more pronounced in fish species with more robust acid-base regulatory mechanisms; however, this hypothesis must be experimentally tested. Future studies should also investigate whether the fish inner ear epithelium can curb otolith overgrowth during prolonged OA exposure, if the long-term response requires changes in NKA and VHA protein abundance, and if species-specific differences exist. Potential mechanisms include a change in the endolymph pH setpoint,

387 modulation of glycoprotein or Ca^{2+} secretion, and engagement of other compensatory
388 mechanisms. Coupled with functional studies (e.g. Radford et al., 2021; Shen et al.,
389 2016), this information will help predict whether the inner ear vestibular and auditory
390 sensory systems of fish will be affected by OA. Furthermore, understanding the
391 mechanisms responsible for otolith biomineralization and overgrowth during OA
392 exposure can help improve the accuracy of otolith-reliant aging techniques in the future
393 ocean.
394
395

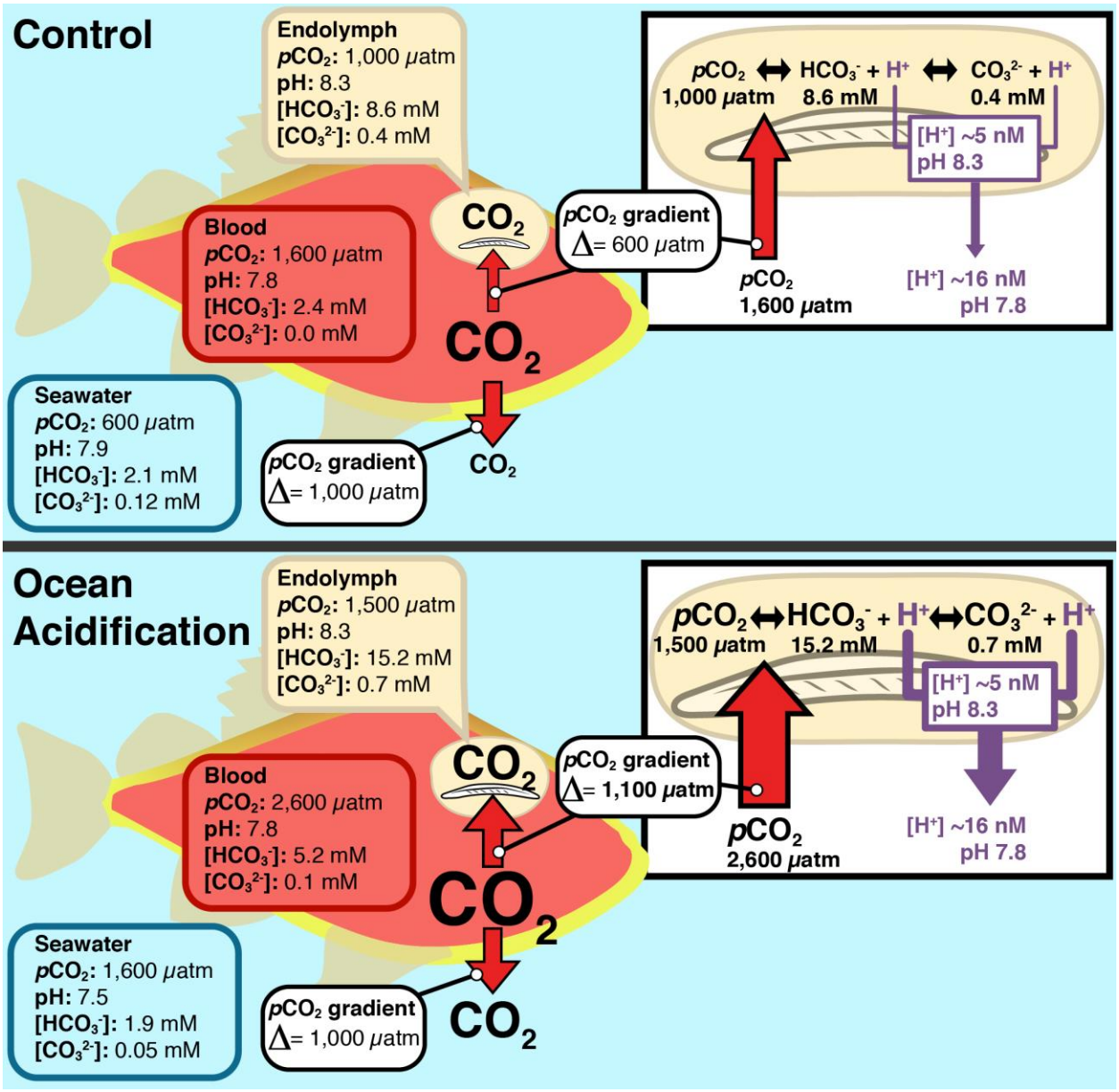

Figure 4: Effect of blood and endolymph acid-base regulation on otolith overgrowth during exposure to ocean acidification. Under control conditions, metabolically produced CO_2 results in higher levels within the fish blood (~1,600 µatm) than those in seawater (~600 µatm) and endolymph (~1,000 µatm). As a result, blood CO_2 diffuses into seawater (Δ = ~1,000 µatm) as it passes through the gills, and into the endolymph (Δ = ~600 µatm) as it passes through the inner ear. Under ocean acidification, the 1,000

μatm increase in seawater pCO_2 (to ~1,600 μatm) induces an equivalent increase in the blood (to ~2,600 μatm), but a lesser increase in the endolymph (to ~1,500 μatm). Thus, the pCO_2 diffusion gradient from the blood into seawater remain constant, but the pCO_2 diffusion gradient from the blood into the endolymph increases (Δ = ~1,100 μatm). This process is driven by pH regulation from the endolymph by the inner ear epithelium, presumably by increased H^+ removal into the blood (although non-bicarbonate buffering cannot be ruled out). The increased CO_2 diffusion rate into the endolymph coupled with endolymph pH regulation results in the accumulation of $[HCO_3^-]$ and $[CO_3^{2-}]$, thereby increasing $\Omega_{aragonite}$ and promoting otolith calcification. The size of the arrows is proportional to the fluxes of CO_2 or H^+.

Acknowledgements

This research was supported by National Science Foundation (NSF) grant IOS #1754994 to M.T, and NSF Graduate Research Fellowship and NSF Postdoctoral Research Fellowship in Biology (award #1907334) to GTK. We thank Phil Zerofski (SIO) for collecting the fish and helping with aquarium matters. We are grateful to Taylor Smith, Shane Finnerty, Gabriel Lopez, Kaelan Prime, and Dr. Till Harter for their help with fish care. We also thank Kaelan Prime and Dr. Till Harter for their assistance with experimental maintenance and sampling.

Bibliography

Bignami, S., Enochs, I.C., Manzello, D.P., Sponaugle, S., Cowen, R.K., 2013. Ocean acidification alters the otoliths of a pantropical fish species with implications for sensory function. Proc. Natl. Acad. Sci. 110, 7366–7370. https://doi.org/10.1073/pnas.1301365110

Bignami, Sean, Sponaugle, S., Cowen, R.K., 2013. Response to ocean acidification in larvae of a large tropical marine fish, *Rachycentron canadum*. Glob. Chang. Biol. 19, 996–1006. https://doi.org/10.1111/gcb.12133

Boutilier, R.G., Heming, T.A., Iwama, G.K., 1984. Appendix: Physicochemical Parameters for use in Fish Respiratory Physiology**The authors were supported by N.S.E.R.C. (Canada), in: Hoar, W.S., Randall, D.J. (Eds.), Fish Physiology. Academic Press, pp. 403–430. https://doi.org/https://doi.org/10.1016/S1546-5098(08)60323-4

Bradford, M.M., 1976. A rapid and sensitive method for the quantitation of microgram quantities of protein utilizing the principle of protein-dye binding. Anal. Biochem. 72, 248–254. https://doi.org/10.1016/0003-2697(76)90527-3

Campana, S.E., 2001. Accuracy, precision and quality control in age determination, including a review of the use and abuse of age validation methods. J. Fish Biol. 59, 197–242. https://doi.org/10.1006/jfbi.2001.1668

Campana, S.E., Neilson, J.D., 1985. Microstructure of Fish Otoliths. Can. J. Fish. Aquat. Sci. 42, 1014–1032.

Campana, S.E., Thorrold, S.R., 2001. Otoliths, increments, and elements: keys to a comprehensive understanding of fish populations? Can. J. Fish. Aquat. Sci. 58, 30–38. https://doi.org/10.1139/cjfas-58-1-30

Checkley, D.M., Dickson, A.G., Takahashi, M., Radich, J.A., Eisenkolb, N., Asch, R., 2009. Elevated CO2 enhances otolith growth in young fish. Science 324, 1683. https://doi.org/10.1126/science.1169806

Culberson, C., Pytkowicz, R.M., 1970. Oxygen-total carbon dioxide correlation in the Eastern Pacific Ocean. J. Oceanogr. Soc. Japan 26, 95–100.

https://doi.org/10.1007/BF02753817
Di Santo, V., 2019. Ocean acidification and warming affect skeletal mineralization in a marine fish. Proc. R. Soc. B Biol. Sci. 286, 20182187. https://doi.org/10.1098/rspb.2018.2187
Esbaugh, A.J., Ern, R., Nordi, W.M., Johnson, A.S., 2016. Respiratory plasticity is insufficient to alleviate blood acid–base disturbances after acclimation to ocean acidification in the estuarine red drum, *Sciaenops ocellatus*. J. Comp. Physiol. B Biochem. Syst. Environ. Physiol. 186, 97–109. https://doi.org/10.1007/s00360-015-0940-6
Esbaugh, A.J., Heuer, R., Grosell, M., 2012. Impacts of ocean acidification on respiratory gas exchange and acid-base balance in a marine teleost, *Opsanus beta*. J. Comp. Physiol. B. 182, 921–934. https://doi.org/10.1016/0034-5687(90)90050-9 http://dx.doi.org/10.1007/s00360-012-0668-5
Faria, A.M., Filipe, S., Lopes, A.F., Oliveira, A.P., Gonçalves, E.J., Ribeiro, L., 2017. Effects of high pCO2 on early life development of pelagic spawning marine fish. Mar. Freshw. Res. 68, 2106. https://doi.org/10.1071/MF16385
Frieder, C.A., Nam, S.H., Martz, T.R., Levin, L.A., 2012. High temporal and spatial variability of dissolved oxygen and pH in a nearshore California kelp forest. Biogeosciences 9, 3917–3930. https://doi.org/10.5194/bg-9-3917-2012
Goodwin, P., Brown, S., Haigh, I.D., Nicholls, R.J., Matter, J.M., 2018. Adjusting Mitigation Pathways to Stabilize Climate at 1.5°C and 2.0°C Rise in Global Temperatures to Year 2300. Earth's Futur. 6, 601–615. https://doi.org/10.1002/2017EF000732
Harter, T.S., Clifford, A.M., Tresguerres, M., 2021. Adrenergically induced translocation of red blood cell β-adrenergic sodium-proton exchangers has ecological relevance for hypoxic and hypercapnic white seabass. Am. J. Physiol. Integr. Comp. Physiol. 1–19. https://doi.org/10.1152/ajpregu.00175.2021
Heuer, R.M., Grosell, M., 2014. Physiological impacts of elevated carbon dioxide and ocean acidification on fish. AJP Regul. Integr. Comp. Physiol. 307, R1061–R1084. https://doi.org/10.1152/ajpregu.00064.2014
Hofmann, G.E., Smith, J.E., Johnson, K.S., Send, U., Levin, L.A., Micheli, F., Paytan,

A., Price, N.N., Peterson, B., Takeshita, Y., Matson, P.G., Crook, E.D., Kroeker, K.J., Gambi, M.C., Rivest, E.B., Frieder, C. a., Yu, P.C., Martz, T.R., 2011. High-frequency dynamics of ocean pH: a multi-ecosystem comparison. PLoS One 6, e28983. https://doi.org/10.1371/journal.pone.0028983

Hurst, T.P., Fernandez, E.R., Mathis, J.T., Miller, J.A., Stinson, C.M., Ahgeak, E.F., 2012. Resiliency of juvenile walleye pollock to projected levels of ocean acidification. Aquat. Biol. 17, 247–259. https://doi.org/10.3354/ab00483

Ishimatsu, A., Hayashi, M., Kikkawa, T., 2008. Fishes in high-CO2, acidified oceans. Mar. Ecol. Prog. Ser. 373, 295–302. https://doi.org/10.3354/meps07823

Kalish, J.M., 1989. Otolith microchemistry: validation of the effects of physiology, age and environment on otolith composition. J. Exp. Mar. Bio. Ecol. 132, 151–178. https://doi.org/10.1016/0022-0981(89)90126-3

Kwan, G.T., Shen, S.G., Drawbridge, M., Checkley, D.M., Tresguerres, M., 2021. Ion-transporting capacity and aerobic respiration of larval white seabass (*Atractoscion nobilis*) may be resilient to ocean acidification conditions. Sci. Total Environ. 791, 148285. https://doi.org/10.1016/j.scitotenv.2021.148285

Kwan, G.T., Smith, T.R., Tresguerres, M., 2020. Immunological characterization of two types of ionocytes in the inner ear epithelium of Pacific Chub Mackerel (*Scomber japonicus*). J. Comp. Physiol. B 190, 419–431. https://doi.org/10.1007/s00360-020-01276-3

Lebovitz, R.M., Takeyasu, K., Fambrough, D.M., 1989. Molecular characterization and expression of the (Na+ + K+)-ATPase alpha-subunit in *Drosophila melanogaster*. EMBO J. 8, 193–202.

Lewis, E., Wallace, D.W.R., 1998. CO2SYS dos program developed for CO2 system calculations.

Liu, X., Patsavas, M.C., Byrne, R.H., 2011. Purification and characterization of meta-cresol purple for spectrophotometric seawater ph measurements. Environ. Sci. Technol. 45, 4862–4868. https://doi.org/10.1021/es200665d

Love, M., Yaklovich, M., Thorsteinson, L., 2002. The Rockfishes of the Northeast Pacific. UC Press, Berkeley.

Mayer-Gostan, N., Kossmann, H., Watrin, A., Payan, P., Boeuf, G., 1997. Distribution of

ionocytes in the saccular epithelium of the inner ear of two teleosts (*Oncorhynchus mykiss* and *Scophthalmus maximus*). Cell Tissue Res. 289, 53–61. https://doi.org/10.1007/s004410050851

Methot, R.D., 2015. Prioritizing Fish Stock Assessments. NOAA Tech. Memo. NMFS-F/SPO- 152, 31 p.

Montgomery, D.W., Kwan, G.T., Davison, W.G., Finlay, J., Berry, A., Simpson, S.D., Engelhard, G.H., Birchenough, S.N.R., Tresguerres, M., Wilson, R.W., 2022. Rapid blood acid-base regulation by European sea bass (*Dicentrarchus labrax*) in response to sudden exposure to high environmental CO2. J. Exp. Biol. https://doi.org/10.1242/jeb.242735

Montgomery, D.W., Simpson, S.D., Engelhard, G.H., Birchenough, S.N.R., Wilson, R.W., 2019. Rising CO2 enhances hypoxia tolerance in a marine fish. Sci. Rep. 9, 1–10. https://doi.org/10.1038/s41598-019-51572-4

Pannella, G., 1971. Fish Otoliths : Daily Growth Layers and Periodical Patterns. Science (80-.). 173, 1124–1127.

Payan, P., De Pontual, H., Bœuf, G., Mayer-Gostan, N., 2004. Endolymph chemistry and otolith growth in fish. Comptes Rendus Palevol 3, 535–547. https://doi.org/10.1016/j.crpv.2004.07.013

Payan, P., Edeyer, A., de Pontual, H., Borelli, G., Boeuf, G., Mayer-Gostan, N., 1999. Chemical composition of saccular endolymph and otolith in fish inner ear: lack of spatial uniformity. Am. J. Physiol. 277, R123–R131.

Payan, P., Kossmann, H., Watrin, a, Mayer-Gostan, N., Boeuf, G., 1997. Ionic composition of endolymph in teleosts: origin and importance of endolymph alkalinity. J. Exp. Biol. 200, 1905–1912.

Pimentel, M.S., Faleiro, F., Dionisio, G., Repolho, T., Pousao-Ferreira, P., Machado, J., Rosa, R., 2014. Defective skeletogenesis and oversized otoliths in fish early stages in a changing ocean. J Exp Biol 217, 2062–2070. https://doi.org/10.1242/jeb.092635

Pisam, M., Payan, P., LeMoal, C., Edeyer, A., Boeuf, G., Mayer-Gostan, N., 1998. Ultrastructural study of the saccular epithelium of the inner ear of two teleosts, *Oncorhynchus mykiss* and *Psetta maxima*. Cell Tissue Res. 294, 261–270.

https://doi.org/10.1007/s004410051176
R Development Core Team, 2013. R: A language and environment for statistical computing. R foundation for statistical computing.
Radford, C.A., Collins, S.P., Munday, P.L., Parsons, D., 2021. Ocean acidification effects on fish hearing. Proceedings. Biol. Sci. 288, 20202754. https://doi.org/10.1098/rspb.2020.2754
Réveillac, E., Lacoue-Labarthe, T., Oberhänsli, F., Teyssié, J.L., Jeffree, R., Gattuso, J.P., Martin, S., 2015. Ocean acidification reshapes the otolith-body allometry of growth in juvenile sea bream. J. Exp. Mar. Bio. Ecol. 463, 87–94. https://doi.org/10.1016/j.jembe.2014.11.007
Shen, S.G., Chen, F., Schoppik, D.E., Checkley, D.M., 2016. Otolith size and the vestibulo-ocular reflex of larvae of white seabass *Atractoscion nobilis* at high pCO2. Mar. Ecol. Prog. Ser. 553, 173–182. https://doi.org/10.3354/meps11791
Shiao, J.C., Lin, L.Y., Horng, J.L., Hwang, P.P., Kaneko, T., 2005. How can teleostean inner ear hair cells maintain the proper association with the accreting otolith? J. Comp. Neurol. 488, 331–341. https://doi.org/10.1002/cne.20578
Takagi, Y., 2002. Otolith formation and endolymph chemistry: A strong correlation between the aragonite saturation state and pH in the endolymph of the trout otolith organ. Mar. Ecol. Prog. Ser. 231, 237–245. https://doi.org/10.3354/meps231237
Takagi, Y., 1997. Meshwork arrangement of mitochondria-rich, Na+,K+-ATPase-rich cells in the saccular epithelium of rainbow trout (*Oncorhynchus mykiss*) inner ear. Anat. Rec. 248, 483–489. https://doi.org/10.1002/(SICI)1097-0185(199708)248:4<483::AID-AR1>3.0.CO;2-N
Takagi, Y., Tohse, H., Murayama, E., Ohira, T., Nagasawa, H., 2005. Diel changes in endolymph aragonite saturation rate and mRNA expression of otolith matrix proteins in the trout otolith organ. Mar. Ecol. Prog. Ser. 294, 249–256. https://doi.org/10.3354/meps294249
Takeshita, Y., Frieder, C.A., Martz, T.R., Ballard, J.R., Feely, R.A., Kram, S., Nam, S., Navarro, M.O., Price, N.N., Smith, J.E., 2015. Including high-frequency variability in coastal ocean acidification projections. Biogeosciences 12, 5853–5870. https://doi.org/10.5194/bg-12-5853-2015

582 Tohse, H., Ando, H., Mugiya, Y., 2004. Biochemical properties and
583 immunohistochemical localization of carbonic anhydrase in the sacculus of the
584 inner ear in the salmon *Oncorhynchus masou*. Comp. Biochem. Physiol. - A Mol.
585 Integr. Physiol. 137, 87–94. https://doi.org/10.1016/S1095-6433(03)00272-1
586 Tohse, H., Murayama, E., Ohira, T., Takagi, Y., Nagasawa, H., 2006. Localization and
587 diurnal variations of carbonic anhydrase mRNA expression in the inner ear of the
588 rainbow trout *Oncorhynchus mykiss*. Comp. Biochem. Physiol. B. Biochem. Mol.
589 Biol. 145, 257–64. https://doi.org/10.1016/j.cbpb.2006.06.011
590 Tresguerres, M., Hamilton, T.J., 2017. Acid-base physiology, neurobiology and
591 behaviour in relation to CO2 -induced ocean acidification. J. Exp. Biol. 220, 2136–
592 2148. https://doi.org/10.1242/jeb.144113
593 Vitale, F., Clausen, L.W., Chonchuir, G.N., 2019. Handbook of fish age estimation
594 protocols and validation methods. ICES Cooperative Research Report No. 346.
595 https://doi.org/10.17895/ices.pub.5221
596

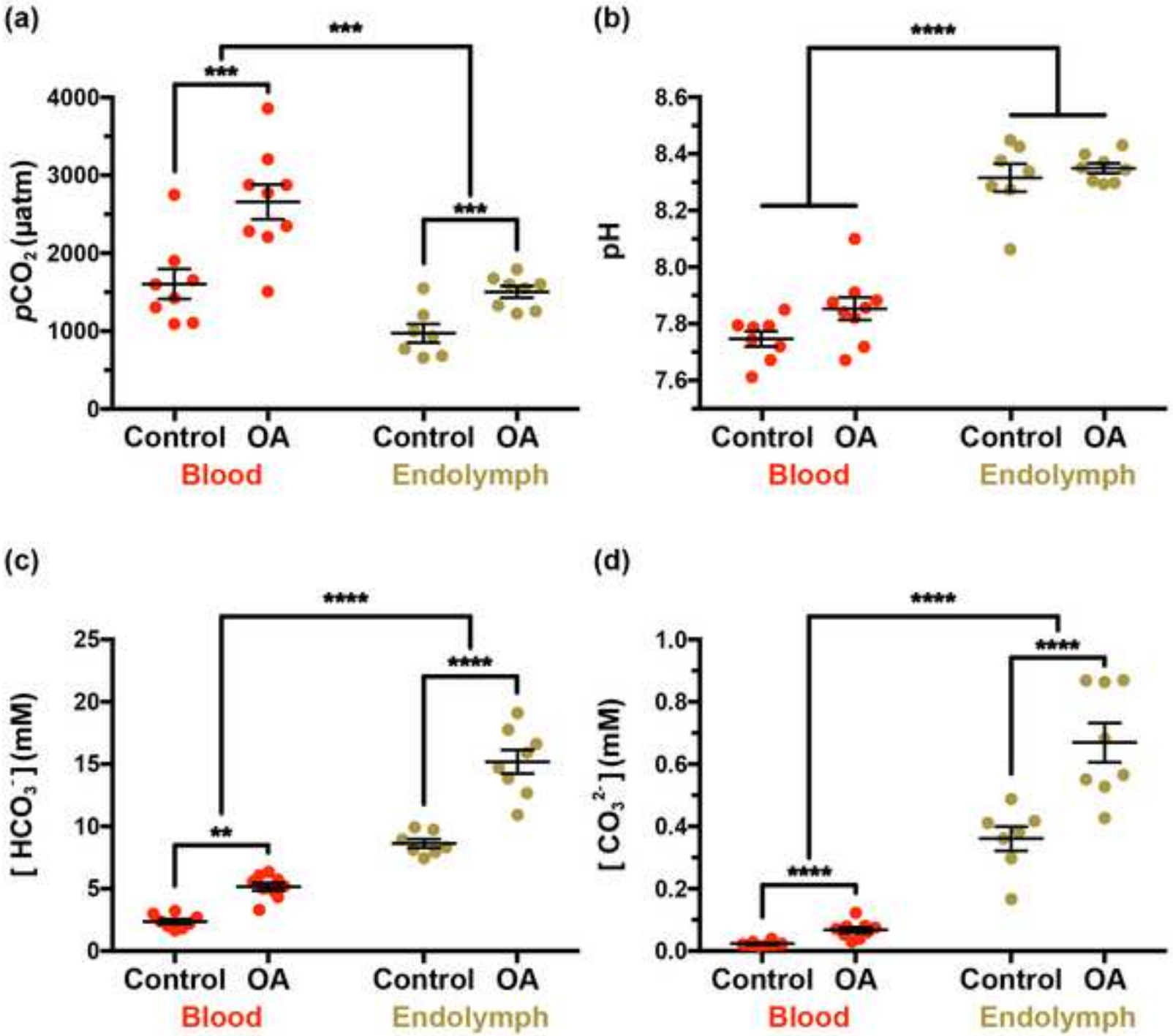

Figure 2 (TIFF)

Click here to access/download;Figure;Figure 2.tif

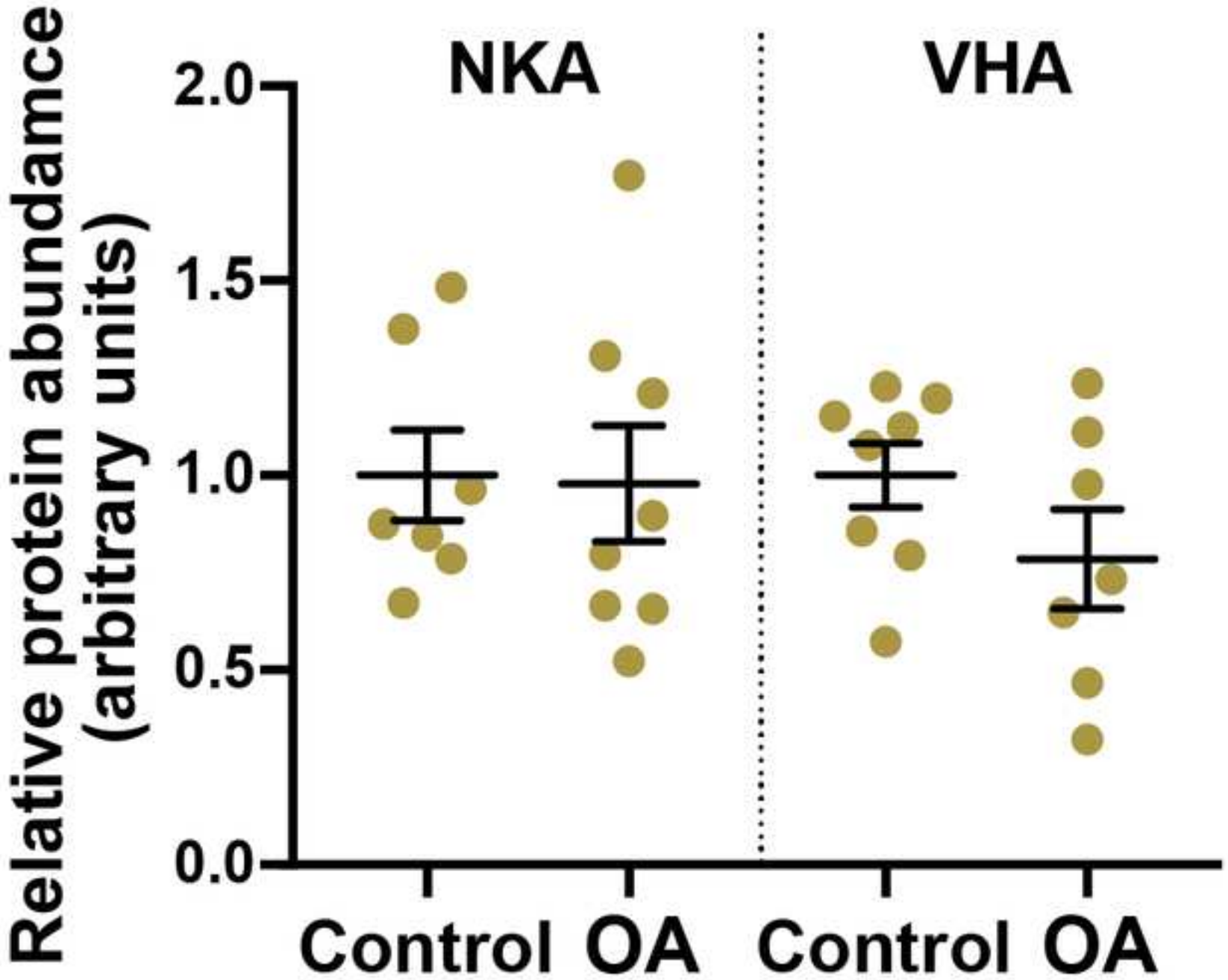

Figure 3 (TIFF) Click here to access/download;Figure;Figure 3.tif

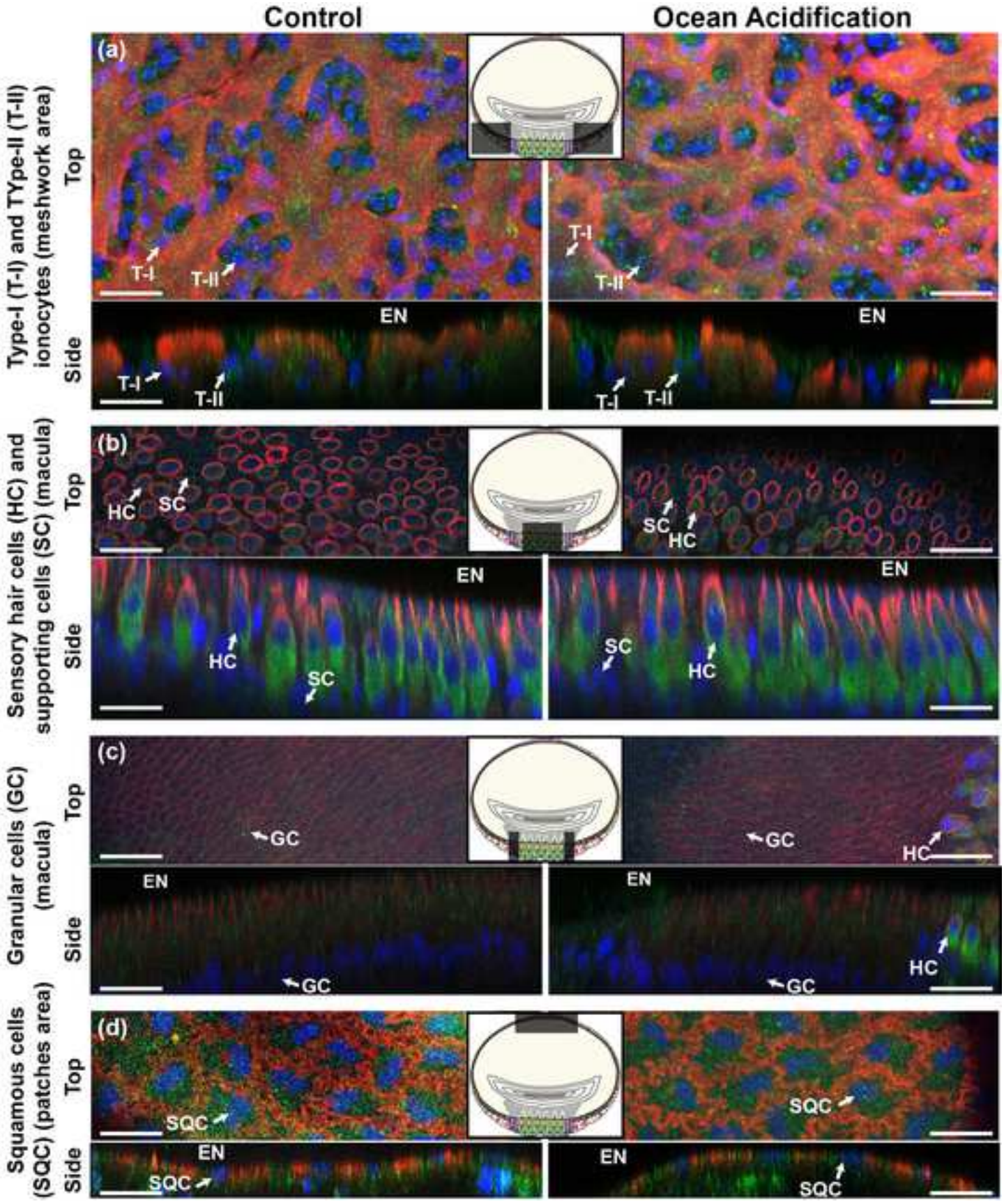

Figure 4 (TIFF)

Click here to access/download;Figure;Figure 4.tif

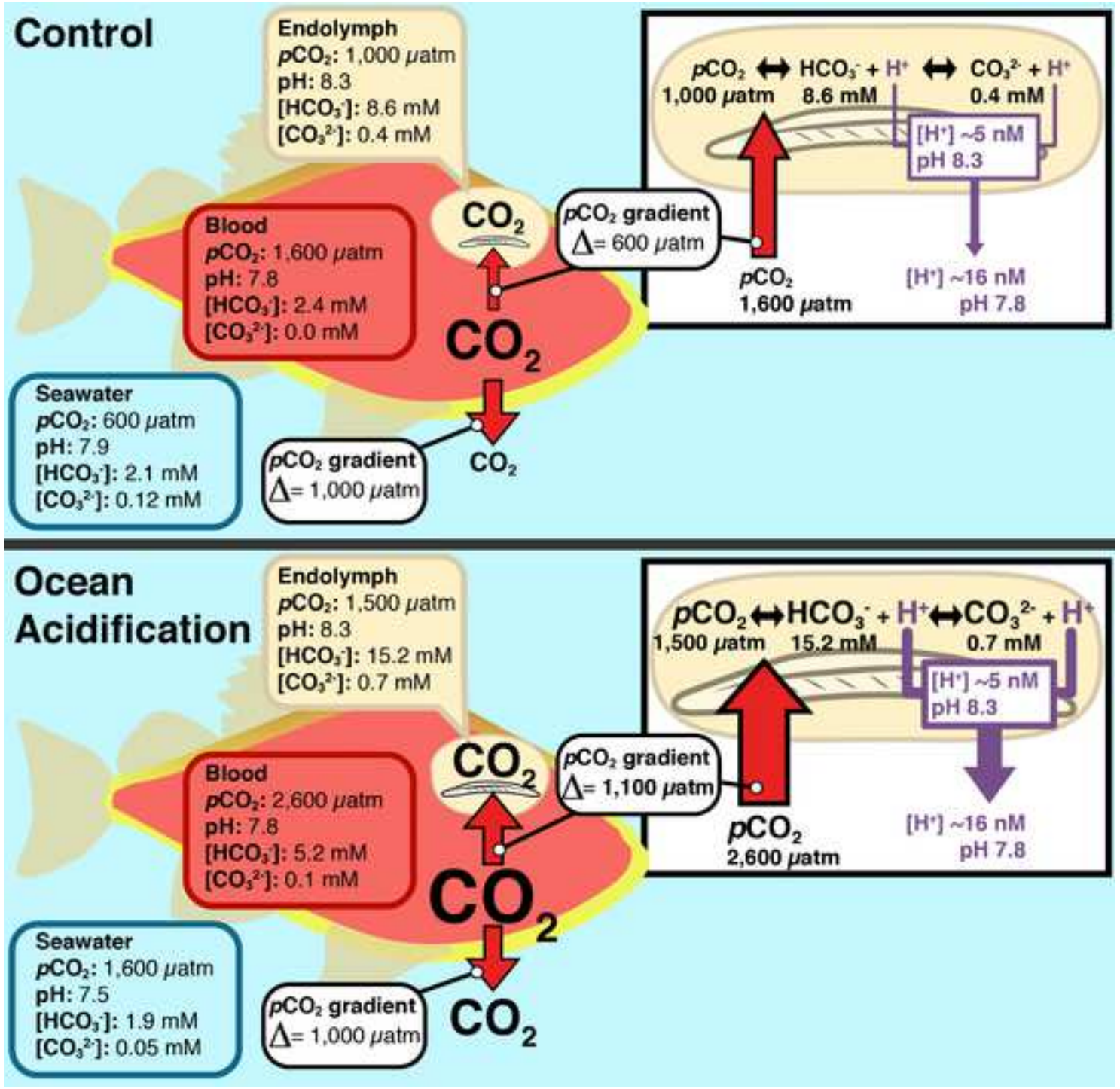

Declaration of Interest Statement

No competing interests declared.

Author contributions

GTK and MT conceived and designed the experiments, analysed the data, and wrote the manuscript. GTK executed the experiments. All authors gave final approval for publication.